Astronomy & Astrophysics manuscript no.
(will be inserted by hand later)

High-resolution X-ray spectroscopy of Procyon by Chandra and XMM-Newton

A.J.J. Raassen[1,2], R. Mewe[1], M. Audard[3], M. Güdel[3], E. Behar[4], J.S. Kaastra[1], R.L.J. van der Meer[1], C.R. Foley[5], and J.-U. Ness[6]

[1] SRON National Institute for Space Research, Sorbonnelaan 2, 3584 CA Utrecht, The Netherlands
[2] Astronomical Institute "Anton Pannekoek", Kruislaan 403, 1098 SJ Amsterdam, The Netherlands
[3] Paul Scherrer Institut, Würenlingen & Villigen, 5232 Villigen PSI, Switzerland
[4] Columbia Astrophysics Laboratory, Columbia University, New York, NY 10027, USA
[5] Mullard Space Science Laboratory, University College London, Surrey, RH5 6NT, United Kingdom
[6] Universität Hamburg, Gojenbergsweg 112, 21029 Hamburg, Germany

Received date February 1, 2008; accepted date . . .

Abstract. We report the analysis of the high-resolution soft X-ray spectrum of the nearby F-type star Procyon in the wavelength range from 5 to 175 Å obtained with the Low Energy Transmission Grating Spectrometer (LETGS) on board Chandra and with the Reflection Grating Spectrometers (RGS) and the EPIC-MOS CCD spectrometers on board XMM-Newton. Line fluxes have been measured separately for the RGS and LETGS. Spectra have been fitted globally to obtain self-consistent temperatures, emission measures, and abundances. The total volume emission measure is $\sim 4.1 \times 10^{50}$ cm^{-3} with a peak between 1 and 3 MK. No indications for a dominant hot component ($T \gtrsim 4$ MK) were found. We present additional evidence for the lack of a solar-type FIP-effect, confirming earlier EUVE results.

Key words. Stars: individual: Procyon, α Canis Minoris – stars: coronae – stars: late-type – stars: activity – X-rays: stars

1. Introduction

Magnetized hot outer atmospheres (coronae) are ubiquitous in cool stars (spectral classes F-M). The particular example of the solar corona has revealed rich details on coronal structures, thermal stratification, abundance patterns, and the physics of heating and mass motion. Nevertheless, in many other stars coronal phenomena not common to the Sun are regularly observed, such as persistent high-density ($n_{\rm e} > 10^{10}$ cm^{-3}) coronal plasmas, persistent very hot gas ($T > 10$ MK), or abundances at variance with solar values (Bowyer et al. 2000). The Sun's relatively modest magnetic activity is representative for a particular evolutionary state of a $1M_{\odot}$ star (Güdel et al. 1997), while most stellar objects regularly observed by X-ray satellites belong either to the more abundant low-mass classes with some exceptional magnetic activity (M dwarfs and young K dwarfs) or to tidally coupled binary systems with strongly enhanced magnetic dynamos (RS CVn or Algol-type binaries).

High-resolution X-ray spectroscopy of such stellar systems now available from Chandra and XMM-Newton (Brinkman et al. 2000, 2001) has revealed coronal features clearly at variance with solar phenomena. However, to translate solar knowledge to stellar environments, it is important to study stars that are relatively similar to the Sun. Given the low X-ray luminosity of such stars, there are only a few in the solar neighborhood accessible to high-resolution X-ray spectroscopy. We present here a detailed analysis of the X-ray spectrum of Procyon, a nearby bright X-ray source with a coronal plasma of about 1–3 MK, exhibiting a cooler X-ray spectrum than magnetically active stars that have predominantly been studied so far with XMM-Newton and Chandra (Audard et al. 2001ab; Güdel et al. 2001ab; Mewe et al. 2001). The late-type (F5 IV-V) optically bright (m_v=0.34) star Procyon (with a faint white dwarf companion) at a distance of 3.5 pc has a line-rich coronal spectrum in the X-ray region. The mass of Procyon is $1.75M_{\odot}$ and its radius $2.1R_{\odot}$ (Irwin et al. 1992). The high-resolution spectrum of Procyon has been studied earlier using EUVE (Drake et al. 1995; Schrijver et al. 1995; Schmitt et al. 1996) and by means of the LETGS on board Chandra (Ness et al. 2001). Ness et al. focussed their efforts on the density-sensitive and temperature-sensitive lines of C V, N VI, and O VII only. Here we present an extended investigation of the LETGS spectrum covering the total spectral range from 5-175 Å together with the analysis of the RGS spectra from 5-37 Å. In Sect. 2 we describe the observations. Sect. 3 (Analysis) is divided into a part on global fitting (3.2) based on the total spectrum and a part that contains consistency checks based on individual line measurements (3.3).

Send offprint requests to: A.J.J.Raassen,
e-mail: a.j.j.raassen@sron.nl

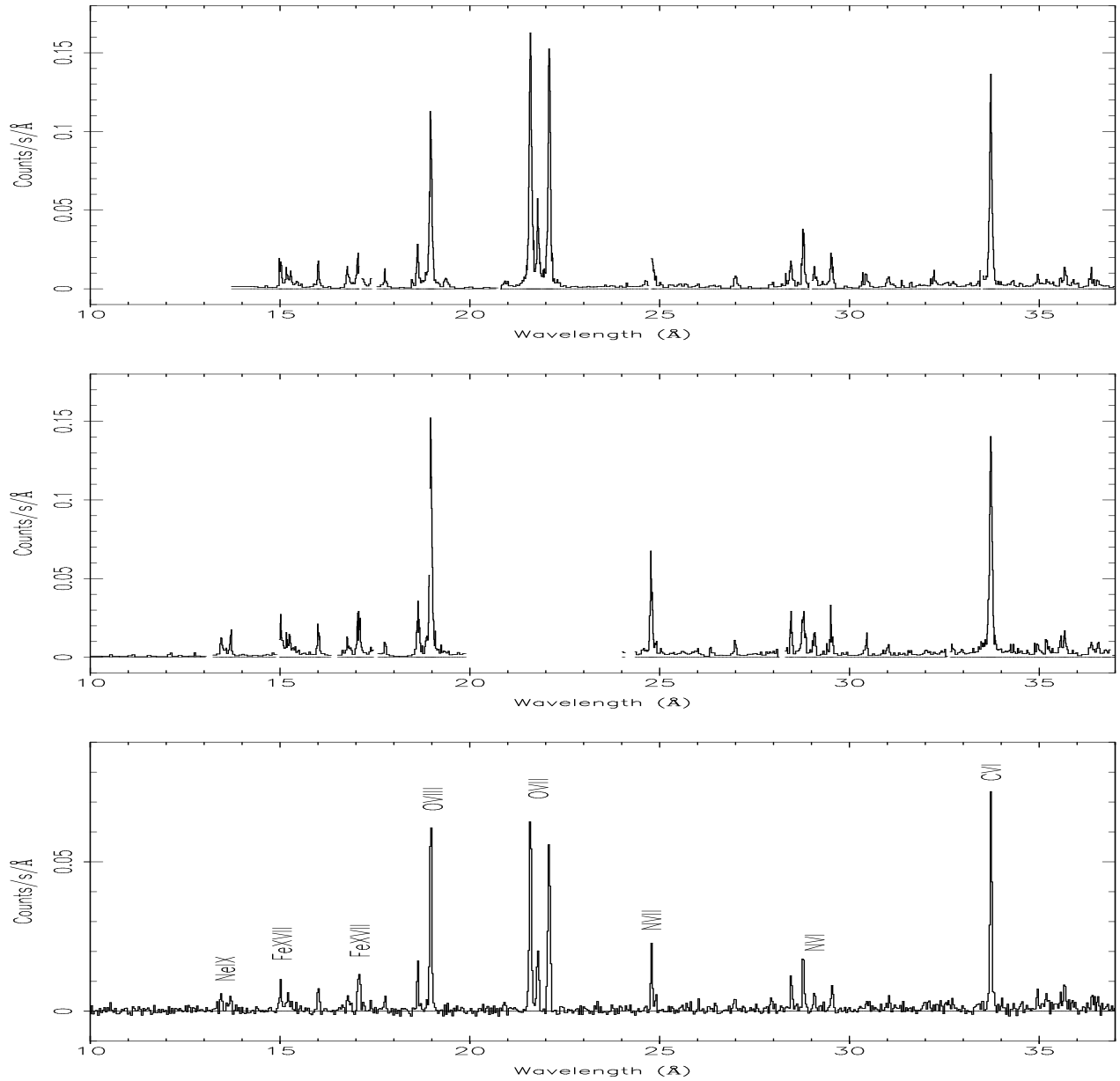

Fig. 1. From top to bottom the spectra of Procyon observed by RGS1, RGS2 and LETGS in the wavelength region from 10 to 37 Å

2. Observations

The spectrum of Procyon was obtained during 70.4 ksec (on November 8, 1999) by the High Resolution Camera (HRC-S) and the LETGS on board Chandra. The HRC-S contains three flat detectors, each 10 cm long. LETGS consists of 180 grating modules. The LETGS spectrum covers the range from 5 to 175 Å. The LETGS spectra were summed over the +1 and -1 orders and contain also the higher orders. The higher orders are fitted in the model calculations, but can be neglected for Procyon. The curve of the effective area as a function of wavelength is complicated because of the presence of absorption edges (e.g., around 42 Å) and gaps between 62–65 Å and 52–56 Å (+1 & –1 order, respectively) due to the gaps between the detector plates. We use the SRON values (based on calibration by van der Meer et al. 2002), which agree within about 5–10% with the CXC values, as given in the Chandra LETGS Calibration Review of 31 Oct. 2001.[1] The wavelength resolution is $\Delta\lambda \sim 0.06$ Å (FWHM). The wavelength uncertainty in the calibration is a few mÅ below 30 Å and about 0.020 Å in the region above 30 Å. The spectra are background subtracted. The statistical errors in the line fluxes include errors from the background. For further instrumental details see also Brinkman et al. (2000).

Later (on October 22, 2000), the spectrum of Procyon was observed by XMM-Newton using the RGS and EPIC-MOS. The total observing time was $\approx$ 107 ksec; however, due to large

[1] http://cxc.harvard.edu/cal/Links/Letg/User/Review_311001/eff_area.html

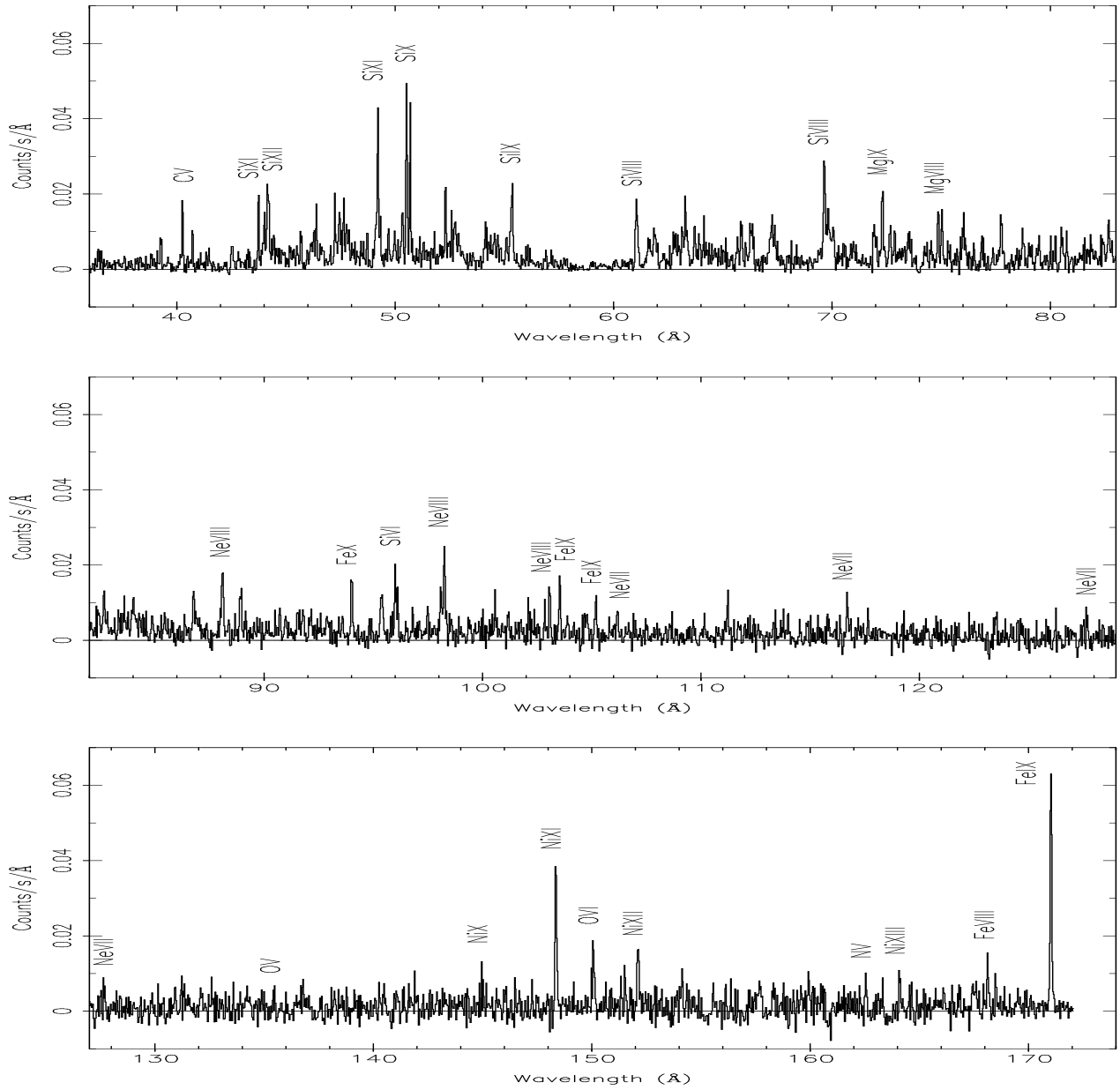

Fig. 2. The Procyon spectrum observed by LETGS in the region 36-174 Å

solar flare activity at the end of the observation, we removed 16.7 ksec of data, leaving a total of 90.5 ksec of "good" data. In XMM-Newton three telescopes focus X-rays onto three EPIC cameras (two MOS and one pn). About half of the photons in the beams of two telescopes (Turner et al. 2001) are diffracted by sets of reflecting gratings and are then focussed onto the RGS detectors. The RGS spectral resolution is $\Delta\lambda \sim 0.07$ Å, with a maximum effective area of about 140 cm^2 around 15 Å. The wavelength uncertainty is 7-8 mÅ. The first spectral order has been selected by means of the energy resolution of the individual CCDs. For further details see den Herder et al. (2001).

The data were processed by the XMM-Newton SAS using the calibration of February 2001. The RGS cover the range from 5 to 37 Å. The EPIC spectra, which have a lower resolution but higher sensitivity, are used to constrain the high-temperature part of Procyon's EM distribution. Because of the high resolution of the grating spectrometers we will focus on the spectra from these instruments. In Fig. 1, we show the RGS spectra together with an extract of the LETGS spectrum covering the wavelength range from 10 to 37 Å. No notable features are observed below 10 Å in the LETGS and RGS spectra. However, the EPIC-MOS detects the H- and He-like lines of Mg. The remaining part of the LETGS spectrum is shown in Fig. 2. From Fig. 1 the gaps in the two RGS spectra due to CCD failure of CCD 7 (RGS1) and 4 (RGS2) are obvious.

3. Analysis

Table 1. Wavelengths and fluxes for RGS1, RGS2, and LETGS, together with the line identifications from MEKAL and KELLY

RGS1		RGS2		LETGS		Line identifications[a]			
λ(Å)	flux[b]	λ(Å)	flux[b]	λ(Å)	flux[b]	MEKAL	flux[c]	KELLY	Ion
gap	—	13.454(9)	0.17(4)	13.450(13)	0.14(5)	13.448	0.14	13.447	Ne IX
gap	—	13.701(6)	0.17(4)	13.690(15)	0.12(5)	13.700	0.10	13.700	Ne IX
15.018(7)	0.20(5)	15.024(9)	0.26(4)	15.015(18)	0.21(6)	15.014	0.16	15.013	Fe XVII[d]
15.176(13)	0.12(3)	15.161(21)	0.08(3)	—	—	15.175	0.03	15.176	O VIII
—	—	—	—	15.207(28)	0.13(5)	—	0.09	—	Fe XVII[e]
15.281(12)	0.11(3)	15.258(12)	0.09(5)	—	—	15.265	0.04	15.260	Fe XVII
16.008(3)	0.17(3)	16.013(9)	0.20(5)	16.008(9)	0.18(5)	16.003	0.15	16.007	O VIII[f]
16.776(9)	0.16(3)	16.776(15)	0.12(4)	16.790(14)	0.13(5)	16.780	0.10	16.775	Fe XVII
17.047(9)	0.23(4)	17.044(14)	0.19(5)	17.054(12)	0.22(9)	17.055	0.12	17.051	Fe XVII
—	—	17.099(12)	0.25(5)	17.102(9)	0.29(9)	17.100	0.10	17.100	Fe XVII
17.402(12)	0.07(3)	17.402(28)	0.06(3)	17.396(17)	0.08(5)	17.380	0.04	17.396	O VII
17.765(9)	0.10(3)	17.772(9)	0.11(4)	17.769(13)	0.14(5)	17.770	0.12	17.768	O VII
18.624(4)	0.30(4)	18.637(6)	0.37(5)	18.629(5)	0.39(8)	18.628	0.39	18.627	O VII
18.970(2)	1.61(8)	18.975(2)	1.78(11)	18.972(2)	1.83(15)	18.973	1.93	18.969	O VIII
20.918(27)	0.04(3)	gap	—	20.905(22)	0.14(7)	20.910	0.06	20.910	N VII
21.596(2)	2.36(11)	gap	—	21.597(2)	3.01(25)	21.602	3.35	21.602	O VII
21.797(4)	0.53(6)	gap	—	21.792(5)	0.90(14)	21.800	0.80	21.804	O VII
22.098(2)	2.20(11)	gap	—	22.089(2)	2.57(23)	22.100	2.33	22.101	O VII
—	—	24.780(3)	0.88(7)	24.790(4)	0.80(14)	24.781	0.76	24.781	N VII
—	—	24.907(22)	0.08(4)	24.906(11)	0.18(9)	24.900	0.08	24.898	N VI
27.001(11)	0.16(4)	26.994(12)	0.14(4)	26.979(19)	0.18(9)	26.990	0.08	26.990	C VI
28.460(7)	0.30(5)	28.465(6)	0.39(6)	28.470(6)	0.49(12)	28.470	0.39	28.466	C VI
28.785(4)	0.69(9)	28.775(6)	0.71(8)	28.785(5)	0.88(15)	28.790	0.77	28.787	N VI
29.078(9)	0.24(5)	29.084(9)	0.29(7)	29.082(12)	0.29(10)	29.090	0.32	29.084	N VI
29.524(6)	0.43(6)	29.520(8)	0.38(6)	29.546(11)	0.43(13)	29.530	0.41	29.534	N VI
30.445(12)	0.20(5)	30.446(13)	0.22(5)	30.450(25)	0.18(11)	30.448	0.22	30.448	Ca XI
31.027(16)	0.18(5)	31.021(12)	0.15(5)	31.054(15)	0.22(10)	31.015	0.19	31.015	Si XII
—	—	33.490(26)	0.15(7)	33.510(18)	0.17(10)	—	—	—	—
33.724(2)	3.49(17)	33.726(2)	4.15(30)	33.731(2)	4.02(32)	33.736	4.64	33.736	C VI
34.967(12)	0.19(6)	34.962(15)	0.17(7)	34.959(15)	0.27(17)	34.970	0.22	34.973	C V
35.198(30)	0.13(6)	35.193(12)	0.27(8)	35.188(18)	0.29(15)	35.212	0.12	35.212	Ca XI
35.566(16)	0.15(7)	35.562(12)	0.26(7)	35.566(16)	0.23(14)	35.576	0.27	35.576	Ca XI
35.682(8)	0.37(8)	35.676(9)	0.38(8)	35.672(9)	0.53(16)	35.665	0.28	35.665	S XIII
36.374(12)	0.35(10)	36.372(15)	0.28(7)	36.399(15)	0.34(14)	36.398	0.25	36.398	S XII
36.544(19)	0.15(6)	36.561(19)	0.29(9)	36.547(15)	0.24(13)	36.563	0.24	36.563	S XII

[a] Identifications for MEKAL (Mewe et al. 1995) and KELLY (Kelly 1987) identical.
[b] Observed flux in 10^{-4} photons/cm^2/s.
[c] Model flux in 10^{-4} photons/cm^2/s, obtained from 3-T fitting of LETGS (see Sect. 3.2).
[d] Fe XVII lines are strongly mixed with Fe XVI satellite lines.
[e] Line not split up; mixture of 15.175 Å and 15.265 Å from O VIII and Fe XVII, respectively.
[f] Small contamination by Fe XVIII possible.
Values in parentheses are statistical 1σ uncertainties in the last digits.

3.1. Detailed analysis of the spectra

The spectral lines from all three instruments have been measured individually. We folded monochromatic delta functions through the instrumental response matrices in order to derive the integrated line fluxes. No additional width was needed to fit the shape of the lines. A constant "background" level was adjusted in order to account for the real continuum and for the pseudo-continuum created by the overlap of several weak, neglected lines. In Table 1, we have collected the measured wavelengths and fluxes of the emission lines in the RGS instruments together with those in the LETGS in the similar wavelength range. The fluxes among the three data sets, as collected in Table 1, are in good agreement in view of the systematic uncertainties in the calibration. However for some lines deviations appear, which are caused by gaps between the individual CCDs. In this wavelength range (below 40 Å) the identification is in general straightforward. The dominating lines are strong and belong to H- and He-like ions for which atomic parameters are well known. Although XMM-Newton and Chandra observed Procyon at different dates no strong differences in flux (Table 1) are noticed, resulting in the conclusion that the coronal emission of Procyon did not vary strongly from one observation to the other.

Table 2 contains the same information as Table 1 for LETGS lines which occur above 37 Å. The extracted fluxes are as measured at Earth. Therefore they are not corrected for interstellar absorption which is of the order of 4% at 100 Å, 6% at 125 Å, 10% at 150 Å, and 15% at 175 Å. We added one Fe line (Fe X at 174.69 Å) that was observed in an offset observation of Procyon (obsID = 1224; 14.8 ksec). For that line the effective area was obtained by extrapolation. The line flux ratio of that line compared to the line at 171.075 Å in the offset observation was used to establish the flux value.

In both tables, we have compared the measured wavelengths with the wavelengths in various atomic databases: the MEKAL (Mewe et al. 1985, 1995) code[2], KELLY (Kelly 1987) and the database of the National Institute of Standards and Technology (NIST), which is also available on the web.[3] We have also compared with a list of lines observed in the solar corona (Doschek & Cowan 1984, hereafter D&C). Further we compare our measured iron lines with the results from laboratory experiments such as the Lawrence Livermore National Laboratory's Electron Beam Ion Trap (EBIT) (see Beiersdorfer et al. 1999 and Lepson et al. 2002 for Fe VIII–X and Lepson et al. 2000 for Fe XII–XIII). A number of lines in Table 2 (see note "d") are in close wavelength agreement to lines identified in EBIT. Finally in Table 1 the fluxes, from the multi-temperature global fitting of Sect. 3.2, have been added.

Some possible line identifications have been omitted from Table 2, due to the absence of comparable lines belonging to the same multiplet or ion (Table 3) or due to ambiguity of the identification of lines in atomic databases (Kelly 1987). The latter concerns lines at 60.989 Å (Si VII, VIII, & IX) and 61.852 Å (Si VIII & IX).

Earlier benchmarks with a solar flare spectrum (Phillips et al. 1999) and with RGS and LETGS spectra of Capella (Audard et al. 2001a; Mewe et al. 2001) have already shown that the current atomic databases are lacking quite a number of spectral lines for L-shell transitions of Ne, Mg, Si, and S, that appear in the long-wavelength region above about 40 Å. This is illustrated by the many identifications present in the third Col. (KELLY), which are absent in MEKAL. For the Fe L-shell Behar et al. (2001) have shown that the HULLAC atomic data are fairly accurate.

3.2. Global Fitting and emission measure modeling

3.2.1. Multi-temperature fitting

We first characterize the thermal structure and the elemental composition of Procyon's corona. To this end, we fitted multi-T models using SPEX (Kaastra et al. 1996a) of the spectra (RGS+MOS and LETGS). For both the observations the calculations require two dominant temperature components. A third (small and not very significant) temperature component is needed to account for the lines of low stages of ionization, present in the LETGS spectrum. The reduced χ^2 is relatively high (1.3–2) for the fits. This is due to a lack of lines

[2] http://saturn.sron.nl/∼kaastra/spex/line.ps.gz

[3] http://physics.nist.gov/cgi-bin/AtData/main_asd

Table 2. Wavelengths and fluxes for LETGS above 36.5 Å, together with the line identifications from MEKAL, KELLY, and D&C

LETGS		Line identifications[a]					
		MEKAL		KELLY		D&C	
λ(Å)	flux[b]	λ(Å)	Ion	λ(Å)	Ion	λ(Å)	Ion
39.276	0.63(14)	39.300	S XI	39.300	S XI	39.30	S XI
				39.264	Si X		
				39.305	Si X		
40.263	2.29(36)	40.270	C V	40.268	C V	40.27	C V
40.718	1.88(42)	40.730	C V	40.731	C V	40.73	C V
41.475	1.07(29)	41.470	C V	41.472	C V	41.47	C V
		41.480	Ar IX	41.480	Ar IX		
42.543	1.29(28)	42.530	S X	42.543	S X	42.53	S X
42.810	0.33(17)	–		42.826	Si XI	–	
43.743	0.54(8)	43.740	Si XI	43.763	Si XI	43.74	Si XI
44.014	0.43(8)	44.020	Si XII	44.021	Si XII	44.02	Si XII
44.150	0.67(10)	44.165	Si XII	44.165	Si XII	44.17	Si XII
44.218	0.52(10)	44.249	Si IX	44.215	Si IX	44.22	Si IX
45.677	0.20(4)	45.680	Si XII	45.692	Si XII	45.68	Si XII
				45.684	Si X		
46.283	0.25(7)	46.300	Si XI	46.300	Si XI	46.30	Si XI
46.391	0.40(8)	46.410	Si XI	46.401	Si XI	46.41	Si XI
47.242	0.46(8)	47.280	Mg X	47.310	Mg X	47.31	Mg X
				47.231	Mg X		
				47.249	S IX	47.25	S IX
47.452	0.48(8)	47.500	S IX	47.433	S IX	47.43	S IX
				47.518	S IX		
				47.453	Si XI		
47.642	0.49(8)	47.654	S X	47.655	S X	47.65	S X
				47.653	Si XI		
47.774	0.34(7)	47.793	S X	47.791	S X	47.79	S X
47.883	0.24(8)	47.896	Mg X	47.905	S X	47.90	Mg X
				47.899	Si XI		
48.720	0.23(6)	48.730	Ar IX	48.73	Ar IX	48.73	Ar IX
49.109	0.33(8)	–		49.119	S IX	49.12	S IX
49.207	1.44(14)	49.220	Si XI	49.222	Si XI	49.22	Si XI
		49.180	Ar IX	49.18	Ar IX	49.18	Ar IX
49.324	0.32(7)	–		49.328	S IX	–	
49.696	0.29(7)	–		49.701	Si X	–	
49.975	0.28(6)	50.019	Si VIII[c]	50.019	Si VIII	–	
50.327	0.51(8)	–		50.333	Si X	–	
50.520	1.68(15)	50.530	Si X	50.524	Si X	50.53	Si X
50.686	1.30(14)	50.690	Si X	50.691	Si X	50.69	Si X
52.306	0.75(11)	52.300	Si XI	52.296	Si XI	52.30	Si XI
52.594	0.35(8)	52.615	Ni XVIII	52.615	Ni XVIII	–	
				52.611	Si IX		
52.715	0.30(7)	52.720	Ni XVIII	52.720	Ni XVIII	52.70	S VIII
52.772	0.30(7)	–		52.756	S VIII	–	
				52.789	S VIII		
52.898	0.30(7)	52.911	Fe XV	52.911	Fe XV	52.87	Fe XV
54.133	0.56(13)	54.118	S VIII	54.118	S VIII	54.12	S VIII
		54.142	Fe XVI	54.142	Fe XVI	54.15	Fe XVI
54.180	0.31(10)	54.180	S IX	54.175	S IX	54.18	S IX
54.546	0.54(13)	–		54.571	Si X	–	
				54.566	S VIII		
54.700	0.45(11)	54.728	Fe XVI	54.728	Fe XVI	54.70	Fe XVI
55.094	0.68(15)	55.060	Mg IX	55.060	Mg IX	55.06	Mg IX
				55.094	Si IX	55.12	Si IX
				55.116	Si IX		
				55.096	Si X		
55.270	0.88(25)	55.272	Si IX	55.272	Si IX	55.27	Si IX
				55.305	Si IX	55.31	Si IX

LETGS		Line identifications[a]					
		MEKAL		KELLY		D&C	
λ(Å)	flux[b]	λ(Å)	Ion	λ(Å)	Ion	λ(Å)	Ion
55.359	2.14(27)	55.356	Si IX	55.356	Si IX	55.36	Si IX
				55.401	Si IX	55.40	Si IX
56.037	0.19(11)	56.000	Ni XIII	56.027	Si IX	56.03	Si IX
				56.081	S IX	56.08	S IX
56.836	0.20(8)	–		56.804	Si X	–	
57.741	0.80(35)	–		57.736	Mg VIII	–	
				57.778	Si IX		
57.856	0.78(35)	57.880	Mg X	57.876	Mg X	57.88	Mg X
		57.920	Mg X	57.920	Mg X	57.92	Mg X
61.020	1.41(25)	61.050	Si VIII	61.019	Si VIII	61.01	Si VIII
				61.038	Mg IX		
61.087	1.38(24)	–		61.070	Si VIII	61.08	Si VIII
				61.088	Mg IX		
61.578	0.52(17)	61.600	S VIII	61.600	S VIII	61.60	S VIII
61.668	0.49(15)	–		61.649	Si IX	61.66	Si IX
61.843	0.67(11)	61.841	Si IX	61.852	Si IX	61.84	Si IX
61.916	0.55(17)	61.912	Si VIII	61.914	Si VIII	61.91	Si VIII
				61.895	Si VIII	61.90	Si VIII
62.748	0.53(17)	62.755	Mg IX	62.751	Mg IX	62.76	Mg IX
		62.699	Fe XIII[d]	62.694	Fe XIII		
62.849	0.38(11)	62.879	Fe XVI	62.879	Fe XVI	62.88	Fe XVI
		62.800	Fe X[d]	62.8	Fe X		
63.161	0.64(13)	63.153	Mg X	63.152	Mg X	63.15	Mg X
63.283	0.94(15)	63.294	Mg X	63.295	Mg X	63.29	Mg X
63.390	0.38(8)	63.314	Mg X	63.304	S VIII	63.40	Mg VII
				63.396	Mg VII		
63.720	0.58(11)	63.719	Fe XVI	63.719	Fe XVI	63.71	Fe XVI
				63.732	Si VIII	63.73	Si VIII
63.921	0.39(10)	–		–		–	
64.135	0.44(11)	–		–		–	
65.677	0.38(11)	65.672	Mg X	65.672	Mg X	65.67	Mg X
65.826	0.49(13)	65.840	Mg X	65.847	Mg X	65.84	Mg X
				65.822	Ne VIII		
65.884	0.41(10)	65.905	Fe XII[d]	65.905	Fe XII	–	
				65.892	Ne VIII	–	
66.057	0.28(10)	66.047	Fe XII[d]	66.047	Fe XII	66.04	Fe XII
66.255	0.64(14)	–		66.259	Ne VIII	–	
66.352	0.63(13)	–		66.330	Ne VIII	–	
67.161	0.48(11)	67.132	Mg IX	67.135	Mg IX	67.13	Mg IX
67.255	0.87(18)	67.233	Mg IX	67.239	Mg IX	67.22	Mg IX
				67.291	Fe XII[d]		
67.375	0.68(14)	67.350	Ne VIII	67.382	Ne VIII	67.35	Ne VIII
69.646	2.03(21)	69.658	Si VIII	69.632	Si VIII	69.66	Si VIII
		69.660	Fe XV	69.66	Fe XV		
69.827	1.05(14)	69.825	Si VIII	69.790	Si VIII	69.83	Si VIII
70.046	0.70(11)	70.020	Si VII	70.027	Si VII	70.03	Si VII
		70.010	Fe XII	70.01	Fe XII		
		70.054	Fe XV	70.054	Fe XV	70.05	Fe XV
71.929	0.69(13	–		71.901	Mg IX	71.92	Mg IX
				71.955	Si VII		
72.034	0.43(13)	72.030	Mg IX	72.027	Mg IX	72.03	Mg IX
72.302	1.44(18)	72.311	Mg IX	72.312	Mg IX	72.31	Mg IX
		72.310	Fe XI	72.310	Fe XI		
72.668	0.73(14)	72.663	S VII	72.663	S VII	72.66	S VII
72.871	0.58(15)	72.850	Fe IX[d]	72.850	Fe IX	–	
73.478	0.47(11)	–		73.470	Ne VIII	–	
		73.471	Fe XV	73.471	Fe XV	73.47	Fe XV
73.555	0.43(11)	73.560	Ne VIII	73.563	Ne VIII	73.56	Ne VIII
74.860	1.10(18)	74.854	Mg VIII	74.858	Mg VIII	74.85	Mg VIII
		74.845	Fe XIII[d]	74.845	Fe XIII		

LETGS		Line identifications[a]					
		MEKAL		KELLY		D&C	
λ(Å)	flux[b]	λ(Å)	Ion	λ(Å)	Ion	λ(Å)	Ion
75.035	1.05(18)	75.034	Mg VIII	75.034	Mg VIII	75.03	Mg VIII
75.978	0.47(11)	76.006	Fe X[d]	76.006	Fe X	76.02	Fe X
76.038	0.77(13)	–		–		–	
76.507	0.32(11)	76.502	Fe XVI	76.502	Fe XVI	76.51	Fe XVI
76.862	0.55(13)	–		–		76.87	Fe XVI
77.740	1.11(18)	77.741	Mg IX	77.737	Mg IX	77.74	Mg IX
78.733	0.71(14)	78.717	Ni XI	78.744	Ni XI	78.72	Ni XI
		78.769	Fe X[d]	78.769	Fe X		
79.483	0.58(13)	79.488	Fe XII	79.488	Fe XII	79.49	Fe XII
80.017	0.38(11)	80.022	Fe XII	80.022	Fe XII	80.02	Fe XII
80.236	0.54(14)	–		80.255	Mg VIII	–	
80.507	0.74(14)	80.501	Si VI	80.501	Si VI	80.50	Si VI
		80.510	Fe XII	80.510	Fe XII	80.51	Fe XII
80.751	0.54(14)	–		80.725	Si VI	–	
81.865	0.42(11)	–		81.895	Si VII	–	
82.420	0.48(11)	82.430	Fe IX[d]	82.430	Fe IX	82.43	Fe IX
82.667	0.97(17)	82.744	Fe XII	82.598	Mg VIII	–	
82.808	0.35(10)	82.837	Fe XII	82.837	Fe XII	–	
				82.822	Mg VIII		
83.337	0.38(11)	–		83.358	Si VI	–	
83.600	0.55(15)	–		83.587	Mg VII	83.59	Mg VII
				83.611	Si VI		
83.764	0.47(17)	83.766	Mg VII	83.766	Mg VII	83.77	Mg VII
83.935	0.46(11)	83.959	Mg VII	83.959	Mg VII	83.96	Mg VII
				83.910	Mg VII	83.91	Mg VII
84.032	0.40(11)	–		84.025	Mg VII	84.02	Mg VII
84.292	0.40(11)	84.292	Ne VII	84.292	Ne VII	84.29	Ne VII
				84.212	Ne VII		
84.433	0.39(11)	–		–		–	
85.448	0.38(11)	–		85.477	Fe XII	85.47	Fe XII
				85.407	Mg VII	85.41	Mg VII
86.765	1.13(17)	86.772	Fe XI	86.772	Fe XI	86.77	Fe XI
86.876	0.55(17)	–		86.847	Mg VIII	–	
87.021	0.46(14)	87.025	Fe XI	87.025	Fe XI	87.02	Fe XI
				87.017	Mg VIII		
88.087	1.68(20)	88.092	Ne VIII	88.092	Ne VIII	88.08	Ne VIII
88.893	0.68(14)	–		–		–	
88.955	0.75(15)	–		88.952	Mg VI	–	
89.156	0.43(13)	89.185	Fe XI	89.185	Fe XI	89.18	Fe XI
90.719	0.59(13)	–		90.708	Mg VII	–	
90.989	0.43(10)	91.009	Fe XIV	91.009	Fe XIV	–	
				90.955	Fe XVII[e]		
91.529	0.52(13)	91.564	Ne VII	91.564	Ne VII	91.56	Ne VII
91.627	0.38(8)	–		–		–	
91.777	0.58(13)	91.808	Ni X	91.790	Ni X	91.81	Ni X
92.155	0.51(13)	–		92.123	Mg VIII	–	
92.858	0.55(14)	–		92.850	Ne VII	–	
93.587	0.58(15)	–		–		–	
94.001	1.70(24)	94.012	Fe X[d]	94.012	Fe X	94.02	Fe X
95.339	0.90(18)	95.374	Fe X	95.374	Fe X	95.37	Fe X
		95.338	Fe X[d]	95.338	Fe X	–	
95.412	1.04(20)	95.483	Mg VI	95.483	Mg VI	95.48	Mg VI
				95.421	Mg VI	95.42	Mg VI
95.997	1.46(20)	–		96.022	Si VI	96.02	Si VI
96.124	0.79(17)	96.122	Fe X[d]	96.122	Fe X	96.12	Fe X
96.804	0.71(18)	96.788	Fe X[d]	96.788	Fe X	–	
97.104	0.34(15)	97.122	Fe X[d]	97.122	Fe X	97.12	Fe X
97.486	0.78(17)	97.502	Ne VII	97.502	Ne VII	97.50	Ne VII
98.091	1.58(25)	98.115	Ne VIII	98.115	Ne VIII	98.13	Ne VIII
98.251	2.89(34)	98.260	Ne VIII	98.260	Ne VIII	98.26	Ne VIII

LETGS		Line identifications[a]					
		MEKAL		KELLY		D&C	
λ(Å)	flux[b]	λ(Å)	Ion	λ(Å)	Ion	λ(Å)	Ion
100.57	1.05(24)	–		100.597	Mg VIII	–	
102.85	0.90(22)	102.91	Ne VIII	102.911	Ne VIII	102.9	Ne VIII
103.07	1.68(27)	103.08	Ne VIII	103.085	Ne VIII	103.1	Ne VIII
103.54	2.08(32)	103.57	Fe IX[d]	103.566	Fe IX	103.6	Fe IX
103.88	0.72(22)	–		–		–	
104.67	0.68(21)	–		–		–	
104.78	0.86(21)	104.81	O VI	104.813	O VI	–	
105.20	1.22(21)	105.21	Fe IX[d]	105.208	Fe IX	105.2	Fe IX
106.18	1.03(20)	106.19	Ne VII	106.192	Ne VII	106.2	Ne VII
111.23	1.49(28)	–		111.198	Ca X	–	
111.71	0.53(13)	111.57	Mg VI	111.552	Mg VI	111.6	Mg VI
		111.72	Mg VI	111.746	Mg VI	111.7	Mg VI
113.33	0.46(11)	–		113.315	Fe VIII	–	
113.77	0.60(20)	–		113.763	Fe VIII	–	
				113.793	Fe IX		
113.99	0.71(20)	–		113.990	Mg V	114.0	Mg V
				114.029	Mg V		
114.54	0.48(14)	–		114.564	Fe VIII	–	
114.88	0.66(17)	–		114.785	Mg V	114.8	Mg V
115.37	0.51(18)	115.33	Ne VII	115.33	Ne VII	–	
		-		115.39	Ne VII	–	
115.80	0.77(20)	115.83	O VI	115.826	O VI	115.8	O VI
115.89	0.46(17)	–		–		–	
116.70	1.54(25)	116.69	Ne VII	116.693	Ne VII	116.7	Ne VII
116.87	0.54(14)	–		–		–	
117.20	0.54(20)	117.20	Fe VIII[d]	117.197	Fe VIII	–	
117.66	0.80(20)	–		–		–	
119.31	0.46(13)	–		–		–	
120.31	0.60(15)	120.33	O VII	120.331	O VII	–	
122.49	0.73(18)	122.49	Ne VI	122.49	Ne VI	122.5	Ne VI
123.54	1.31(31)	–		–		–	
124.51	0.98(25)	–		–		–	
126.25	0.98(32)	–		126.280	Mg V	–	
127.53	0.98(25)	–		–		–	
127.69	1.44(29)	127.66	Ne VII	127.663	Ne VII	127.7	Ne VII
129.86	1.07(34)	129.83	O VI	129.871	O VI	129.9	O VI
130.92	1.78(39)	130.94	Fe VIII[d]	130.941	Fe VIII	130.9	Fe VIII
131.21	1.78(35)	131.24	Fe VIII[d]	131.240	Fe VIII	131.2	Fe VIII
134.21	1.43(41)	–		–		–	
135.48	0.97(35)	135.52	O V	135.523	O V	135.5	O V
136.78	1.91(53)	–		–		–	
140.27	1.36(49)	–		–		–	
141.04	0.79(22)	141.04	Ca XII	141.038	Ca XII	141.0	Ca XII
144.97	1.73(49)	144.99	Ni X	144.988	Ni X	145.0	Ni X
147.27	1.12(35)	147.27	Ca XII	147.278	Ca XII	147.3	Ca XII
148.36	11.3(10)	148.40	Ni XI	148.402	Ni XI	148.4	Ni XI
150.08	5.08(60)	150.10	O VI	150.1	O VI	150.1	O VI
151.52	2.36(39)	–		151.548	O V	–	
152.11	5.60(66)	152.15	Ni XII	152.153	Ni XII	152.2	Ni XII
154.14	2.73(42)	154.18	Ni XII	154.175	Ni XII	154.2	Ni XII
155.56	1.36(28)	–		–		–	
156.14	1.66(32)	–		156.140	Ne V	–	
156.38	1.29(31)	–		–		–	
157.68	2.76(42)	157.73	Ni XIII	157.730	Ni XIII	157.7	Ni XIII
158.33	2.08(35)	158.38	Ni X	158.377	Ni X	158.4	Ni X
158.78	1.47(34)	–		158.770	Ni XIII	–	
159.24	1.03(27)	–		159.300	Si X	159.1	Ar XIII
159.58	1.83(43)	–		–		–	
159.93	3.09(43)	159.94	Ni X	159.977	Ni X	159.9	Ni X
		159.97	Ni XIII	159.97	Ni XIII		

LETGS		Line identifications[a]					
		MEKAL		KELLY		D&C	
λ(Å)	flux[b]	λ(Å)	Ion	λ(Å)	Ion	λ(Å)	Ion
162.56	2.94(83)	162.56	N V	162.556	N V	–	
164.11	3.53(74)	164.15	Ni XIII	164.146	Ni XIII	164.1	Ni XIII
167.43	3.9(10)	167.49	Fe VIII	167.486	Fe VIII	167.5	Fe VIII
167.59	3.9(12)	167.66	Fe VIII	167.656	Fe VIII	–	
168.13	7.4(13)	168.17	Fe VIII	168.172	Fe VIII	168.2	Fe VIII
168.51	5.4(13)	168.54	Fe VIII	168.545	Fe VIII	168.5	Fe VIII
168.90	5.0(18)	168.93	Fe VIII	168.929	Fe VIII	168.9	Fe VIII
171.04	114(8)	171.08	Fe IX	171.075	Fe IX	171.1	Fe IX
174.49	118(24)	174.53	Fe X	174.53	Fe X	174.5	Fe X

[a] from MEKAL (Mewe et al. 1995), KELLY (1987), and D&C (solar line list of Doschek and Cowan 1984).
[b] Observed flux in 10^{-4} photons/cm^2/s with in parentheses 1σ uncertainty in the last digits.
[c] MEKAL placed it at 52.0 Å.
[d] line identified in EBIT spectrum.
[e] from CHIANTI (Dere et al. 1997).

Table 3. Possible line identifications left out of Table 2. Col. λ: observed wavelengths from Table 2. Cols. 2 and 3 give a possible identification which has not been given in Table 2, due to the absence of the lines, given in Cols. 4 and 5

λ(Å)	present	ion	missing	ion
93.587	93.616	FeVIII	93.469	FeVIII
			108.077	FeVIII
98.583	98.548	FeVIII	98.371	FeVIII
103.88	103.937	FeXVIII	93.923	FeXVIII
103.88	103.904	MgV	110.859	MgV

in the MEKAL code and to the high resolution of the instrument. Small wavelength deviations (about 1-2 bins i.e. 0.02-0.04 Å) between lines in the spectrum and in the model are often present (see Table 2). This effect results in a sharp maximum and minimum in the value of the normalized difference between model and observation around the peak of the line (see also Fig. 4). The results of RGS and LETGS are very similar.
In Table 4 results for temperatures T (in MK), emission measures EM, and abundances are given. Statistic 1σ uncertainties are given in parentheses. The emission measure is defined as $EM = n_{\rm e} n_{\rm H} V$, where V is the volume contributing to the emission and for solar abundances the hydrogen density $n_{\rm H} \simeq 0.85 n_{\rm e}$. The temperatures and emission measures of all spectra show a dominant region between 1 and 2.5 MK. The two dominant temperature components are about 1.2 and 2.3 MK. Using EUVE, Schmitt et al. (1996) derived a DEM with a peak temperature of 1.6 MK based on Fe-lines only. This is in satisfactory agreement with our results.

The total emission measures summed over all temperature components are about $4.6(.4) \times 10^{50}$ cm^{-3} for LETGS and $3.9(.3) \times 10^{50}$ cm^{-3} for RGS+MOS. These are similar to the total EM of 4.5×10^{50} cm^{-3} found by Schmitt et al. (1996).

The determination of abundances is complicated by several factors. The many weak L-shell lines, which are absent in the atomic code (see difference between Col. "MEKAL" and

"KELLY" of Table 2) can produce a "pseudo-continuum" (see e.g. Fig. 2a between 42 and 58 Å), which bias the determination of the real but very weak continuum. Several fits to the LETGS spectrum were made: a) to the total spectrum, b) to the total spectrum with selected lines in the wavelength range from 40 to 100 Å, to limit the influence of the inaccuracy of atomic data of Ne-, Mg-, and Si- L-shell lines, and c) to a line spectrum with lines of Table 1 and lines with a statistical significance $\gtrsim 4\sigma$ in the wavelength range above 40 Å (see Table 5). During our investigations the absolute (relative to H) abundances turned out to be very sensitive to the selected group of elements introduced in the fit procedure. This is especially true for the elements Ar and Ca. For these reasons no consistent absolute values of the abundances could be obtained. However, abundance ratios turn out to be much more robust. Therefore the abundance values are normalized to oxygen, and are given relative to their solar photospheric values (Anders & Grevesse (1989)), except for iron. For Fe we use log A_{Fe} is 7.51 (see Drake et al. 1995) instead of 7.67 (Anders & Grevesse 1989). Here log A_{Fe} is the logarithmic of the Fe-abundance relative to log A_H=12.0. The abundances presented in Table 4 are derived assuming the same abundances for the three temperature components. These are averaged over the different fits, together with their least-squares-fit standard deviations (within parentheses).

We obtain abundance values between 0.7 and 2.4 relative to Oxygen (e.g., some enhancement for Ne and Si). However, apart from statistical errors these values are also sensitive to systematic errors, due to changes in values of the solar photospheric abundances, where uncertainties of a factor of 2 cannot be excluded (e.g., Prieto et al. 2001; Grevesse & Sauval 1998). So we cannot obtain indications for a significant FIP effect (enhancement of elements with a low First Ionization Potential) as found for the solar corona (e.g., Feldman et al. 1992). This confirms the conclusions by Drake et al. (1995), based on relative abundances from EUVE observations. The abundances of C and N, relative to O are somewhat higher than the values obtained in the solar photosphere (Anders & Grevesse 1989). In the EUVE observations by Drake et al. (1995) no suitable C- and N-lines were present to constrain (relative) abundances.
Values for n_e, given in Table 4, have been obtained by fitting to the O VII and N VI triplet lines. The C V lines have been omitted from this procedure because their intensities are sensitive for the stellar UV-radiative field, mimicing higher densities (Ness et al. 2001; Porquet et al. 2001).

Table 4. Best-fit parameters for a 3-T CIE model fit. Elemental abundances for the three instruments are given normalized to oxygen and relative to solar photospheric values given by Anders & Grevesse (1989), except for Fe[a]. 1σ uncertainties are given in brackets

Parameter	LETGS	RGS+MOS
log $N_{\rm H}$ [cm^{-2}]	18.06[b]	18.06[b]
T_1 [MK]	0.63(.10)	—
T_2 [MK]	1.21(.07)	1.65(.15)
T_3 [MK]	2.26(.12)	2.68(.22)
EM_1 [10^{50}cm^{-3}]	0.41(.14)	—
EM_2 [10^{50}cm^{-3}]	2.45(.27)	3.0(.20)
EM_3 [10^{50}cm^{-3}]	1.72(.29)	0.9(.18)
n_{e2}[10^{10}cm^{-3}]	$1.4\ ^{+1.5}_{-0.6}$	$1.5^{+2.0}_{-0.6}$
n_{e3}[10^{10}cm^{-3}]	$0.2\ ^{+0.8}_{-0.2}$	—
O/H	0.68(0.38)	0.76(0.33)
C/O	1.38(.24)	1.45(.29)
N/O	1.33(.10)	1.47(.5)
O/O	1.0	1.0
Ne/O	1.49(.21)	1.53(.27)
Mg/O	1.1(.5)	—
Si/O	1.56(.36)	—
S/O	0.69(.15)	—
Fe/O	0.97(.31)	1.47(.22)
Ni/O	2.39(.27)	—

[a] In logarithmic units, with
log$_{10}$H=12.00;C=8.56;N=8.05;O=8.93;Ne=8.09;Mg=7.58;
Si=7.55;S=7.21;Ar=6.56;Ca=6.36;Fe=7.51 (see text);Ni=6.25.
[b] see Linsky et al. (1995).

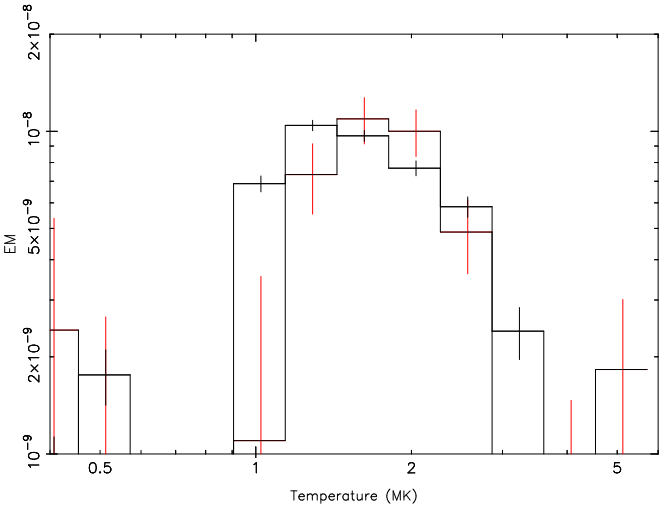

Fig. 3. EM ($n_e n_H V$ in $10^{64} m^{-3}$) for RGS (red) and LETGS (black), using the regularisation algorithm. The relative abundances given in Table 4 have been applied

3.2.2. Temperature dependent emission measure modeling

To show the connectivity of the different temperature components we applied a differential emission measure (DEM) model of Procyon's corona using the various inversion techniques offered by SPEX (see Kaastra et al. 1996b). We applied the abundances obtained in Sect. 3.2.1. In Fig. 3 we give the results based on the regularisation method. Other inversion methods (smoothed clean, or polynomial) give statistically comparable results. The DEM modeling has been applied separately to RGS+MOS and to LETGS.

As a result we find a dominant emission measure of the order of 10^{50} cm^{-3} between 1-3 MK. The total emission measures are $3.5(.3) \times 10^{50}$ cm^{-3} for RGS+MOS and $4.5(.2) \times 10^{50}$ cm^{-3} for LETGS (in line with the multi-temperature fit-

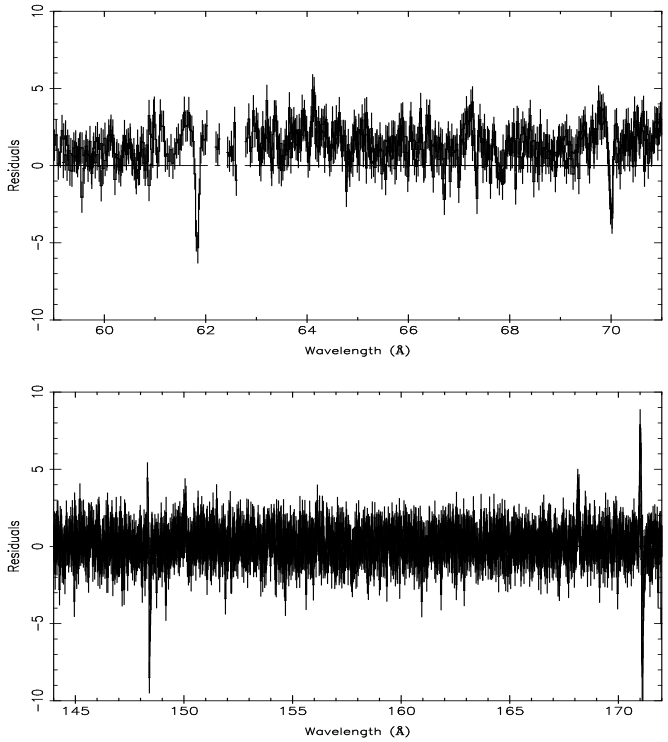

Fig. 4. Fit residuals ((observed - model)/error) of parts of the LETGS spectrum

ting). Fig. 3 allows us to conclude that there is no significant amount of EM at $T \gtrsim 4$ MK in the corona of Procyon. Schmitt et al. (1996) give an upper limit of 6 MK, based on EUVE observations. The EM observed at different times as well as lines fluxes in Table 1 show no significant variability.

Fig. 4 shows fit residuals of parts of the LETGS spectrum fitted using this temperature-dependent emission measure modeling, i.e. applying the model of Fig. 3 (LETGS). From Fig. 4a we recognize large deviations in residual due to model insufficiencies and a pseudo-continuum (most fit residuals positive) due to the lack of weaker lines in current atomic databases in this wavelength range. Clear from Fig. 4b are the succeeding large positive and negative residuals around 148 and 171 Å, due to wavelength deviations of lines in the spectrum and the model.

3.3. Consistency checks using individual lines

The question is whether the model insufficiencies influence our conclusions about temperatures, emission measures, and abundances as obtained in Sect. 3.2. Therefore we have also compared observed and model line fluxes. The advantage of this individual line approach is that we can select strong and unblended lines, for which the theoretical emissivities are quite well established.

For the short-wavelength region this is done for all lines (Table 1), while for the longer wavelength range only lines with a statistical significance $\gtrsim 4\sigma$ were used. For the latter the fluxes have been compared with the 3-T model as well as with the results from the DEM model. The values are given in

Table 5. Observed line fluxes and fluxes obtained from the emissivity from the model

LETGS		Line identifications			
Observed		Model			
λ(Å)	flux[a]	λ(Å)	3-T flux[b]	DEM-flux[b]	Ion
18.972	1.83(15)	18.973	1.93	1.80	N VII
21.597	3.01(25)	21.602	3.35	2.94	N VII
24.790	0.80(14)	24.781	0.76	0.70	N VII
33.731	4.02(32)	33.736	4.64	4.19	C VI
40.263	2.29(36)	40.270	2.03	1.40	C V
40.718	1.88(42)	40.730	1.33		C V
41.475	1.07(29)	41.470	0.68		C V
		41.480	0.28	0.31	Ar IX
43.743	0.54(8)	43.740	0.54	0.94	Si XI
44.150	0.67(10)	44.165	0.64	0.66	Si XII
47.242	0.46(8)	47.280	0.19	0.17	Mg X
47.452	0.48(8)	47.500	0.61	0.60	S IX
47.642	0.49(8)	47.654	0.20	0.31	S X
49.207	1.44(14)	49.220	0.43	0.95	Si XI
		49.180	0.41	0.37	Ar IX
50.520	1.68(15)	50.530	1.48	1.55	Si X
50.686	1.30(14)	50.690	1.50	1.58	Si X
52.306	0.75(11)	52.300	0.45	0.74	Si XI
61.020	1.41(25)	61.050	2.51	1.98	Si VIII
61.087	1.38(24)				Si VIII[c]
63.283	0.94(15)	63.294	1.07	0.93	Mg X
69.646	2.03(21)	69.658	0.85	0.67	Si VIII
		69.660	1.14	1.11	Fe XV
74.860	1.10(18)	74.854	0.51	0.57	Mg VIII
		74.845	0.26	0.40	Fe XIII
75.035	1.05(18)	75.034	0.52	0.57	Mg VIII
77.740	1.11(18)	77.741	0.42	0.37	Mg IX
86.765	1.13(17)	86.772	0.71	0.45	Fe XI
88.087	1.68(20)	88.092	2.33	1.62	Ne VIII
98.251	2.89(34)	98.260	3.02	2.37	Ne VIII
105.20	1.22(21)	105.21	0.32	0.19	Fe IX
130.92	1.78(39)	130.94	0.29	0.20	Fe VIII
131.21	1.78(35)	131.24	0.41	0.29	Fe VIII
148.36	11.3(10)	148.40	11.0	15.5	Ni XI
150.08	5.08(60)	150.10	2.8	2.63	O VI
152.11	5.60(66)	152.15	2.9	6.0	Ni XII
167.43	3.9(10)	167.49	3.9	2.64	Fe VIII
167.59	3.9(12)	167.66	4.0	2.74	Fe VIII
168.13	7.4(13)	168.17	0.3	0.20	Fe VIII
168.51	5.4(13)	168.54	2.0	1.42	Fe VIII
168.90	5.0(18)	168.93	1.3	0.71	Fe VIII
171.04	114(8)	171.08	100	78	Fe IX

[a] Observed flux in 10^{-4} photons/cm^2/s with in parentheses 1σ uncertainty in the last digits.
[b] Model flux in 10^{-4} photons/cm^2/s.
[c] Sum of two Si VIII lines to be compared with model flux.

Table 5. This table shows generally a good agreement between the observed flux and the 3-T flux and the flux from the DEM-modeling, summed over the T-bins. Most striking are the deviations for the Fe VIII lines around 131 and 168 Å. This is definitely due to a large deficiency in the atomic data used. From atomic physics grounds the line at 168.13 Å is the stronger, as

observed in the spectrum and in laboratory experiments (Wang et al. 1984), but in our code this line turns out to be the weakest.[4] Another interesting feature is the contamination of the forbidden C V line - which is often used for density diagnostics - with Ar IX. Another clear example of blending is the line at 74.860 Å which contains Mg VIII and Fe XIII.

We have measured line ratios of density-sensitive He-like triplets from the LETGS and RGS spectra, taking into account the photo-exciting UV flux (Porquet et al. 2001). Our results are consistent in both instruments ($n_{\rm e} \approx 10^{10}$ cm^{-3}) and similar to those of Ness et al. (2001) and our values given in Table 4. These results are also comparable to values obtained by Schrijver et al. (1995) and Schmitt et al. (1996) and to values for the Sun (Drake et al. 2000).

4. Conclusions

The RGS and LETGS spectra of the corona of Procyon below 40 Å are dominated by the H- and He-like transitions of C, N, and O and by Fe XVII lines. Above 40 Å the LETGS spectrum shows many L-shell lines of e.g., Ne, Mg, and Si, together with lines of Fe VIII-XIII of which the Fe IX line at 171.075 is very prominent. All methods applied in Sect. 3.2 to the spectra of the RGS+MOS and the LETGS show temperatures of the corona of Procyon between 1–3 MK. No indication for a considerably higher temperature component ($T \gtrsim 4$ MK) is found. The total EM obtained using RGS and LETGS is about $4.1(.5) \times 10^{50}$ cm^{-3}. The EM distribution shows a smooth continuous structure without separated peak structures. Our results improve on those of Schmitt et al. (1996) who obtain an EM distribution with a maximum temperature around 1.6 MK and a cutoff beyond 6.3 MK. No significant variability of the coronal conditions took place between the observations by RGS and LETGS.

The abundances of C and N, relative to O are somewhat higher ($\sim$ factor 1.5) than the values obtained in the solar photosphere (Anders & Grevesse 1989). The Fe abundance is about 1–1.5 $\times$ solar. No significance for a FIP effect, as observed in the solar corona (Feldman et al. 1992), is found. The same was concluded by Drake et al (1995), based on EUVE observations. This result is an exception of the trends found by Audard et al. (2001c) for RS CVn systems and by Güdel et al. (2001c) for solar analogs. These authors have found indications for the evolution from an inverse FIP effect for highly active stars - via the absence of a FIP effect in intermediately active stars - towards a normal FIP effect for less active stars. Clearly, the weakly active star Procyon does not fit into this picture.

Acknowledgements. The Space Research Organization Netherlands (SRON) is supported financially by NWO. The PSI group acknowledges support from the Swiss National Science Foundation (grant 2100-049343). We are grateful to the calibration teams of the instruments on board XMM-Newton and Chandra. We thank Nancy Brickhouse and Jeremy Drake for their efforts to obtain a long LETGS observation. Finally, we are grateful to the referee for helpful comments.

[4] Recent calculations for Fe VIII by Griffin et al. (2000) give for our observed Fe VIII ratio 131/168=0.14 a temperature of $\sim$ 2.5 MK, near the high-energy limit of the DEM distribution.

References

Anders, E., & Grevesse, N. 1989, Geochimica et Cosmochimica Acta, 53, 197
Audard, M., Behar, E., Güdel, M., et al. 2001a, A&A, 365, L329
Audard, M., Güdel, M., & Mewe, R. 2001b, A&A, 365, L318
Audard, M., Güdel, M., Sres, A. et al. 2001c, in Stellar Coronae in the Chandra and XMM-Newton Era, F. Favata, J.J. Drake (eds.), ASP Conf. Series
Behar, E., Cottam, J., & Kahn, S. M. 2001, ApJ, 548, 966
Beiersdorfer, P., Lepson, J. K., Brown, G. V., et al. 1999, ApJ, 519, L185
Bowyer, S., Drake. J. J., & Vennes, S. 2000, ARA&A, 38, 231
Brinkman, A. C., Behar E., Güdel, M., et al. 2001, A&A, 365, L324
Brinkman, A. C., Gunsing, C. J. T., Kaastra, J. S., et al. 2000, ApJ, 530, L111
Dere, K. P., Landi, E., Mason, H. E., et al. 1997, A&AS, 125, 149
Doschek, G. A., & Cowan, R. D. 1984, ApJS, 56, 67
Drake, J. J., Laming, J. M., & Widing, K. G. 1995, ApJ, 443, 393
Drake, J. J., Peres, G., Orlando, G., et al. 2000, ApJ, 545, 1074
Feldman, U., Mandelbaum, P., Seely, J. F., et al. 1992 ApJS, 81,387
Grevesse, N., & Sauval, A. J. 1998, Space Sci. Rev., 85. 161
Griffin, D.C., Pindzola, M.S., & Badnell, N.R., 2000, A&AS, 142, 317
Güdel, M., Audard, M., Briggs, K., et al. 2001a, A&A, 365, L336
Güdel, M., Audard, M., Magee, H., et al. 2001b, A&A, 365, L344
Güdel, M., Audard, M., Mewe, R. et al. 2001c, in Stellar Coronae in the Chandra and XMM-Newton Era, F. Favata, J.J. Drake (eds.), ASP Conf. Series
Güdel, M., Guinan, E. F., & Skinner, S. L. 1997, ApJ, 483, 947
den Herder, J. W., Brinkman, A. C., Kahn, S. M., et al. 2001, A&A, 365, L7
Irwin, A. W., Fletcher, J. M., Yang, S. L. S., et al. 1992, PASP, 104, 489
Kaastra, J. S., Mewe, R., Liedahl, D. A., et al. 1996b, A&A, 314, 547
Kaastra J. S., Mewe R., Nieuwenhuijzen H. 1996a, in UV and X-ray Spectroscopy of Astrophysical and Laboratory Plasmas, K. Yamashita, T. Watanabe (eds.), Universal Academy Press, Inc., Tokyo, p. 411 (SPEX)
Kelly, R. L. 1987, Atomic and Ionic Spectrum lines below 2000 Angstroms: Hydrogen through Krypton, J. Phys. Chem. Ref. Data 16, suppl. 1
Lepson, J. K., Beiersdorfer, P., Brown, G. V., et al. 2000, RevMexAA (Serie de Conferencias), 9, 137
Lepson, J. K., Beiersdorfer, P., Brown, G. V., et al. 2002, ApJ, submitted
Linsky, J. L., Diplas, A., Wood, B. E., et al. 1995, ApJ, 451, 335
Meer, R.L.J. van der, et al. 2002, in preparation
Mewe, R., Gronenschild, E. H. B. M., & van den Oord, G. H. J. 1985, A&AS, 62, 197
Mewe, R., Kaastra, J. S., & Liedahl, D. A. 1995, Legacy 6, 16 (MEKAL)
Mewe, R., Raassen, A. J. J., Drake, J. J., et al. 2001, A&A, 368, 888
Ness, J.-U., Mewe, R., Schmitt, J. H. M. M., et al. 2001, A&A, 367, 282
Phillips, K. J. H., Mewe, R., Harra-Murnion, L. K., et al. 1999, A&AS, 138, 381
Porquet, D., Mewe, R., Dubau. J., et al. 2001, A&A, 376, 1113
Prieto, C. A., Lambert, D. L., & Asplund, M. 2001, ApJ, 556, L63
Schmitt, J. H. M. M., Drake, J. J., Haisch, B. M., et al. 1996, ApJ, 467, 841

Schrijver, J., Mewe, R., van den Oord, G. H. J., et al. 1995, A&A, 302, 438
Turner, M. J. L., Abbey, A., Arnaud, M., et al. 2001, A&A, 365, L27
Wang, J.-S., Datla, R. U., & Griem, H. R., 1984, Phys. Rev. A, 29, 1558